RESEARCH ARTICLE

Key Points:
- NMR cannot be used to separate mobile and less-mobile porosities for transport
- Electrical resistivity is a diagnostic tool to evaluate pore connectivity
- Complex conductivity responses are not related to solute diffusion length scales

Correspondence to:
R. D. Swanson,
ryaswans@mymail.mines.edu

Anomalous solute transport in saturated porous media: Relating transport model parameters to electrical and nuclear magnetic resonance properties

Ryan D. Swanson[1], Andrew Binley[2], Kristina Keating[3], Samantha France[2], Gordon Osterman[3], Frederick D. Day-Lewis[4], and Kamini Singha[5]

[1]Hydrologic Science and Engineering Program, Colorado School of Mines, Golden, Colorado, USA, [2]Lancaster Environment Centre, Lancaster University, Bailrigg, Lancaster, UK, [3]Department of Earth and Environmental Sciences, Rutgers University Newark, Newark, New Jersey, USA, [4]U.S. Geological Survey, Office of Groundwater, Branch of Geophysics, Storrs, Connecticut, USA, [5]Department of Geology and Geological Engineering and Department of Civil and Environmental Engineering, Hydrologic Science and Engineering, Colorado School of Mines, Golden, Colorado, USA

Abstract The advection-dispersion equation (ADE) fails to describe commonly observed non-Fickian solute transport in saturated porous media, necessitating the use of other models such as the dual-domain mass-transfer (DDMT) model. DDMT model parameters are commonly calibrated via curve fitting, providing little insight into the relation between effective parameters and physical properties of the medium. There is a clear need for material characterization techniques that can provide insight into the geometry and connectedness of pore spaces related to transport model parameters. Here, we consider proton nuclear magnetic resonance (NMR), direct-current (DC) resistivity, and complex conductivity (CC) measurements for this purpose, and assess these methods using glass beads as a control and two different samples of the zeolite clinoptilolite, a material that demonstrates non-Fickian transport due to intragranular porosity. We estimate DDMT parameters via calibration of a transport model to column-scale solute tracer tests, and compare NMR, DC resistivity, CC results, which reveal that grain size alone does not control transport properties and measured geophysical parameters; rather, volume and arrangement of the pore space play important roles. NMR cannot provide estimates of more-mobile and less-mobile pore volumes in the absence of tracer tests because these estimates depend critically on the selection of a material-dependent and flow-dependent cutoff time. Increased electrical connectedness from DC resistivity measurements are associated with greater mobile pore space determined from transport model calibration. CC was hypothesized to be related to length scales of mass transfer, but the CC response is unrelated to DDMT.

1. Introduction

The classical advection-dispersion equation (ADE) consistently fails to match breakthrough curve (BTC) data in many experimental settings. This failure has led to arguments, in part, for better parameterization of effects caused by unresolved heterogeneity [*Berkowitz et al.*, 2006]. New experimental methods focused on hydraulic conductivity, K (m s^{-1}), have demonstrated centimeter-scale vertical resolution using direct-push technologies [*Butler et al.*, 2007; *Liu et al.*, 2009, 2010a, 2013; *Dogan et al.*, 2011; *Bohling et al.*, 2012], yet the ADE may fail at predicting solute transport even if the velocity field is well known [*Major et al.*, 2011]. Tailing, or elevated late-time concentrations relative to predictions based on the ADE, is observed at many field sites but cannot be easily explained even with an extensive understanding of the K field; consequently, temporally and/or spatially nonlocal models have been developed to explain these non-Fickian observations [*Berkowitz et al.*, 2002, 2006; *Salamon et al.*, 2007; *Neuman and Tartakovsky*, 2009; *Zheng et al.*, 2010; *Bianchi et al.*, 2011; *Benson et al.*, 2013]. Determining the parameters for these conceptual models from material properties, without subjecting the material to tracer tests, is desirable but remains speculative [*Benson et al.*, 2001; *Schumer et al.*, 2003; *Reeves et al.*, 2008; *Zhang et al.*, 2009].

Here, we seek to identify mechanisms influencing non-Fickian transport that we can infer using geophysical methods, focusing on properties that may be more readily quantified by material characterization than K,

such as pore structure. The role of the pore structure is critical for anomalous transport: some pore space serves as a solute sink at the early times of tracer tests, and later the slow release from this pore space drives non-Fickian transport including tailing. We focus on the commonly used single-rate dual-domain mass-transfer (DDMT) model, for which model parameters should be measureable—we note that other nonlocal transport schemes also exist. The less-mobile porosity accounts for unresolved geologic heterogeneities below the characteristic measurement scale, including regions of low permeability at the field scale [*Feehley et al.*, 2000; *Harvey and Gorelick*, 2000; *Liu et al.*, 2010b; *Flach*, 2012], or regions where transport is dominated by diffusion into intragranular pore space [*Rao et al.*, 1980a, 1980b, 1982; *Wood et al.*, 1990; *Harmon and Roberts*, 1994; *Ewing et al.*, 2012]. The less-mobile porosity may capture, store, and release solutes, resulting in non-Fickian transport. Unfortunately, direct sampling of less-mobile pore space is difficult without destructive coring and testing; new methods are needed to characterize and infer on this pore space.

Conventional sampling methods, including in-well measurements, are expensive, invasive, and only provide high-resolution measurements in the vertical direction. Geophysical measurements including proton nuclear magnetic resonance (NMR), direct-current (DC) resistivity, and complex conductivity (CC) are thought to be sensitive to the pore structure and arrangement [*Singha et al.*, 2007; *Slater*, 2007; *Dlubac et al.*, 2013; *Keating and Falzone*, 2013], and these geophysical properties may also be related to transport properties important to quantifying nonlocal transport. These geophysical methods, including NMR and DC resistivity, allow for a noninvasive approach to quantify the variability of the subsurface and can be collected at the field scale without the need for time-consuming, invasive tracer tests. We hypothesize that: (1) NMR will provide identification of mobile versus less-mobile fractions of the pore space based on its ability to map "bound" and "unbound" fluids [e.g., *Allen et al.*, 2000; *Westphal et al.*, 2005]; (2) DC resistivity is sensitive to the connectivity of current pathways through both mobile and less-mobile domains, and is thus a potential indicator for solute mass transfer between these regions [e.g., *Swanson et al.*, 2012]; and (3) complex conductivity relaxation times are associated with ion diffusion length scales along grain surfaces [e.g., *Binley et al.*, 2010] and may, therefore, be associated with solute diffusion times in less-mobile regions. These geophysical measurements may be sensitive to hydrogeologic parameters such as K, but here we focus on the pore structure as a possible control for non-Fickian transport that can be measured.

To test these hypotheses we: (1) analyze porous media (the zeolite clinoptilolite) with traditional laboratory material characterization methods, specifically scanning electron microscope (SEM), X-ray computed tomography (CT), and mercury (Hg) porosimetry; (2) collect static DC resistivity, NMR, and CC measurements on our materials; (3) perform column-scale tracer experiments in zeolites as well as a synthetic glass-bead reference material that does not exhibit non-Fickian solute transport; (4) estimate DDMT parameters through calibration to a transport model of BTC data; and (5) use geophysical measurements as diagnostic tools to identify properties influencing non-Fickian transport that drive ADE-based models to perform poorly. In particular, we focus on characterizing the pore structure, including the intergranular and intragranular pore space, with geophysical measurements that are sensitive to the pore environments in saturated porous media to determine whether the fitted DDMT parameters can be described by geophysical measurements. We aim to identify relations between geophysical properties and DDMT parameters such that transport characteristics may be evaluated while avoiding invasive and time-intensive tracer tests. In the absence of such relations, we aim to show the limitations of geophysical methods for estimates of DDMT parameters.

2. Theory and Background

Here, we provide background information for the DDMT model, the geophysical methods, and material characterization tools used in this analysis.

2.1. The DDMT Model
Two equations are necessary to describe the single-rate DDMT model, including one to describe bulk transport, and another to describe solute exchange into and out of the less-mobile domain. The form presented by *van Genuchten and Wierenga* [1976] is:

$$\theta_m \frac{\partial C_m}{\partial t} + \theta_{lm} \frac{\partial C_{lm}}{\partial t} = \theta_m D \frac{\partial^2 C_m}{\partial x^2} - \theta_m v \frac{\partial C_m}{\partial x}, \tag{1a}$$

$$\theta_{lm}\frac{\partial C_{lm}}{\partial t}=\alpha(C_m-C_{lm}),\tag{1b}$$

where t is time (s), x is the spatial coordinate (m), θ_m and θ_{lm} are the mobile and less-mobile porosities (or domains) (-), respectively; C_m and C_{lm} are the concentration in the corresponding θ_m and θ_{lm} (kg m^{-3}); D is the dispersion coefficient (m^2 s^{-1}); v is the average pore water velocity (m s^{-1}) and α is the first-order mass-transfer rate coefficient (s^{-1}). This formulation is for a 1-D, spatially invariant pore-water velocity and dispersion coefficient—a reasonable assumption for laboratory experiments on a homogeneously packed column. We note that there are two subtly different formulations of α found in the literature [*Ma and Zheng*, 2011]. The difference is a consequence of dividing through by the dimensionless porosity term in equation (1b), where the "alternate" α is the product of the "classic" α and θ_{lm}. Here, we use the "alternate" form as implemented in STAMMT-L [*Haggerty*, 2009].

Advection may occur in θ_{lm}, but we assume advection rates in θ_{lm} are much smaller than in θ_m. Therefore, we advocate the term "less-mobile" instead of "immobile" to avoid confusion with a completely disconnected pore space, θ_{dc} (-), that does not significantly contribute to transport or solute exchange but may contribute to electrical and gravimetric measurements. The behavior of this porosity to contribute to hydraulic or electric response depends on the percolation threshold and the arrangement of the pore space [*Wempe and Mavko*, 2001].

The multirate mass-transfer (MRMT) model [*Haggerty and Gorelick*, 1995; *Haggerty et al.*, 2000] is a DDMT model that allows for a distribution of α. The MRMT is more geologically reasonable because multiple scales of heterogeneity are expected in natural media [*Neuman and Di Federico*, 2003]. Many multirate distributions are possible and produce nonunique BTC responses; consequently, we work within a single-rate DDMT model but interpret our results knowing a distribution of α is probable.

2.2. Damköhler Numbers

Not all experimental conditions may result in tailing. The relative timescales of advection to solute exchange between domains is given by the *Damköhler* number, *DaI* [*Bahr and Rubin*, 1987]:

$$DaI=\frac{\alpha\left(1+\frac{\theta_{lm}}{\theta_m}\right)L}{v},\tag{2}$$

where L (m) is the distance away from the source where the solute concentration is measured. Mass transfer is controlled by either slow advection or diffusion, depending on the *DaI* and Peclet numbers [*Zinn et al.*, 2004], and tailing may be due to either diffusion into intragranular pores or exchange between preferential flow paths and θ_{lm} [*Scheibe et al.*, 2013].

Solutes have insufficient time to enter into θ_{lm} if the advection timescale is relatively small compared to the timescale of mass transfer (e.g., under strong pumping), and little mass transfer may be observed. Conversely, for large advection timescales, C_m and C_{lm} will remain in approximate equilibrium and little mass transfer will be observed. The effects of mass transfer are most important for *DaI* near unity. Consequently, in a single-rate model, the best fit α may correspond to a *DaI* of near unity; however, tailing may be present for many experimental conditions due to MRMT. Each α in a multirate distribution will have a corresponding *DaI* for a given θ_{lm}, with some *DaI*s near unity [*Haggerty et al.*, 2004]. As a result, tailing is commonly observed at different flow rates (varying v) and/or observations lengths (varying L).

2.3. Material Characterization

We consider three different material characterization methods to analyze the pore structure of the zeolites: SEM, X-ray CT, and Hg porosimetry. We use SEM images and CT scans to provide qualitative information of the surface pore structures, and use Hg porosimetry to quantify the pore-size distributions [see *Giesche*, 2006].

2.4. Nuclear Magnetic Resonance (NMR)

Proton NMR measurements are sensitive to atoms with unpaired protons or neutrons, which possess a nuclear spin angular momentum. The application of a secondary oscillating field moves the spins out of alignment with the static field; when the secondary field is released the spins return to equilibrium, emitting

a measureable signal. The transverse component (with respect to the static field) of the NMR signal, $I(t)$, is described by a multiexponential decay

$$I(t) = I_0 \sum_i f_i e^{-t/T_{2i}},$$ (3)

where I_0 is the initial signal magnitude, i corresponds to each pore component, and f_i is the fraction of protons relaxing with a relaxation time, T_{2i} (s). I_0 is directly proportional to the number of protons relaxing in the measured volume, and thus water content. The sample's water volume can be estimated from I_0 using an instrument-specific calibration factor, and the total porosity can be determined by adjusting for the sample volume. The relaxation time distribution is given as f_i versus T_{2i}. Assuming fast diffusion and homogeneous applied magnetic fields, the ith relaxation time value is given by [*Senturia and Robinson*, 1970; *Brownstein and Tarr*, 1979]:

$$1/T_{2i} \sim \rho_{2i}/\alpha_i,$$ (4)

where a_i is the characteristic length scale (m) of the ith water-filled pore and ρ_{2i} reflects the capacity of the pore surface to enhance relaxation. The T_2-distribution has been shown to correspond to the pore-size distribution for saturated porous media including the following: sandstone and carbonate cores [*Straley et al.*, 1987; *Arns*, 2004]; silica gels [*Valckenborg et al.*, 2001]; fused glass beads [*Straley et al.*, 1987]; and unconsolidated sand and glass beads [*Hinedi et al.*, 1993; *Bird et al.*, 2005].

In petroleum applications, NMR relaxation time distribution is used to distinguish different porosity regimes. The "producible" porosity, i.e., the porosity containing extractable fluids, can be distinguished from capillary-bound porosity by summing the relaxation time distribution above and below $T_{2cutoff}$ (s), an empirically defined cutoff time [*Timur*, 1969]; consequently, there might be reason to believe NMR could be used to map mobile and less-mobile porosities for DDMT systems. One issue, however, is that the value of $T_{2cutoff}$ is based in practice on pumping rates and rock type [*Allen et al.*, 2000]. The cutoff time may be experiment-specific: in carbonate cores $T_{2cutoff}$ ranges from ~24 ms to greater than 400 ms [*Westphal et al.*, 2005]; in sandstone cores, a 33 ms $T_{2cutoff}$ is commonly used to distinguish producible from capillary-bound porosity, and a 3 ms $T_{2cutoff}$ has been used to determine the clay-bound porosity.

We postulate that NMR may provide an independent method for approximating θ_m and θ_{lm}. Large intragranular pores associated with larger NMR relaxation times are expected to be active in advective transport and thus correspond to θ_m. Smaller intragranular pores associated with smaller NMR relaxation time scales may not contribute to advective transport and correspond to θ_{lm}. We estimate θ_{lm} and θ_m using the NMR signal from $\theta_{lm} = \sum_{T_{2i} < T_{2cutoff}} f_i$ and $\theta_m = \sum_{T_{2i} > T_{2cutoff}} f_i$, respectively. However, the cutoff time used to divide the total porosity into either θ_{lm} or θ_m is not well defined; the empirical cutoff time of 33 ms was weakly supported by a previous study [*Swanson et al.*, 2012].

2.5. Direct-Current (DC) Resistivity

DC resistivity typically requires four electrodes to collect a measurement, including two electrodes to drive electrical current and two electrodes to measure the resultant electrical potential difference. Ohm's law is used to estimate the resistance, R (Ω), and the apparent bulk resistivity, ρ_b (Ω m), is estimated as follows:

$$\rho_b = k \cdot R$$ (5)

where k (m) is a geometric factor is controlled by the position of the electrodes and sample geometry. The inverse of ρ_b is the bulk apparent electrical conductivity, σ_b (S m^{-1}). Static DC resistivity methods have been used to estimate pore-volume and grain-surface conductivity, the formation factor, F (-), and clay content [*Archie*, 1942; *Klein and Sill*, 1982; *Revil et al.*, 1999]. F relates σ_b and fluid conductivity, σ_f (S m^{-1}):

$$\sigma_b = \frac{1}{F} \cdot \sigma_f + \sigma_s$$ (6)

where σ_s (S m^{-1}) is the surface conductivity. *Revil and Cathles* [1999] advocate that F can be used as an inverse measure of the effective porosity, θ_{eff}, i.e.,

$$F \cong \frac{1}{\theta_{eff}}$$ (7)

F is defined by the total porosity and the cementation exponent, m (-), as given by:

$$m = -\frac{\log F}{\log \theta_{tot}} \qquad (8)$$

A value of 1.5 for m represents the analytical solution for perfectly packed glass spheres [*Sen et al.*, 1981] and m is typically greater than 1.5 for consolidated media. We define the total gravimetric porosity, θ_{tot} (-), as the sum of θ_{lm}, θ_m, and θ_{dc}. While θ_{dc} may be disconnected from transport, it may be electrically active [*Wempe and Mavko*, 2001]. The electrical tortuosity, ζ (-), depends on the arrangement of the pore space, and is defined as the product of F and θ_{tot} [*Walsh and Brace*, 1984; *Nelson*, 1994]:

$$\zeta = F \cdot \theta_{tot}. \qquad (9)$$

Even though the fluid-flow tortuosity and electrical tortuosity are not identical [*Zhang and Knackstedt*, 1995], we expect the electrical tortuosity to be associated with fluid-flow tortuosity and both tortuosities to be dependent on the pore structure. The inverse of the formation factor is called the electrical connectedness, G (-), which describes the availability of transport pathways [*Glover*, 2009, 2010]:

$$G = \frac{1}{\zeta} \theta_{tot}. \qquad (10)$$

We focus on G as a measure of the electrical connectivity within the porous medium and assume that the total porosity is the same as the gravimetric porosity, implying that θ_{dc} is electrically active.

2.6. Complex Conductivity (CC)

Complex electrical conductivity (σ^*) is a measure of a porous medium's ability to transport and store charge and consists of a real and imaginary component. The real component (σ_b) of σ^* represents the transport of charge under the influence of an electric field, whereas the imaginary component (commonly σ'') is caused by polarization mechanisms. CC provides information about charge storage, which is typically attributed to processes occurring at or near the grain surface; as a result, CC may offer useful information about pore (or grain) surface area [*Börner et al.*, 1996; *Slater and Lesmes*, 2002]. CC has been increasingly used for near-surface geophysical imaging including estimation of permeability [*Slater and Lesmes*, 2002; *Slater*, 2007; *Revil and Florsch*, 2010; *Titov et al.*, 2010; *Zisser et al.*, 2010], but has yet to be interpreted for DDMT systems.

The magnitude of σ_b and the phase shift between injected current and measured voltage signals can be converted to real and imaginary conductivity components. The CC spectrum is obtained by injecting current at different frequencies (typically in the range 1 mHz to 1 kHz). The spectrum of imaginary conductivity may be interpreted as a result of different electrical relaxation times caused by the diffusion of ions, bound to the material's charged surface, back to their state of equilibrium following cessation of an applied electrical field. The long relaxation times may be sensitive to grain size because the dominant relaxation time, τ_r (s), for polarization along a grain's boundary is related to the grain radius, R_g [m] [*Schwarz*, 1962]:

$$\tau_r = \frac{R_g^2}{2D^*} \qquad (11)$$

where D^* (m^2 s^{-1}) is a diffusion coefficient.

The CC relaxation times reflect the length scale (e.g., the grain boundary or pore length) of the polarization and a diffusion coefficient, which is controlled by the mobility of ions along the surface of the grain. The distribution of CC relaxation times provides insight into the length scales of intragranular electrical diffusion. Interpreted for DDMT systems, we hypothesize that these length scales of intragranular electrical diffusion may be related to length scales of diffusive mass transfer as solute ions are exchanged between mobile and less-mobile domains [*Binley et al.*, 2010]. The length scales of diffusive mass transfer are related to mass-transfer rate coefficients, so CC may provide laboratory estimates of α if this relation between electrical diffusion and solute diffusion length scales exists.

3. Methods

We selected two different samples of the zeolite clinoptilolite for column experiments, referred to as zeolite A and zeolite B. Zeolite A consists of 0.25–2 mm grains, and zeolite B consists of 2–4.8 mm grains (Figure 1). Although both clinoptilolite, the two zeolites were formed at different locations and thus may have
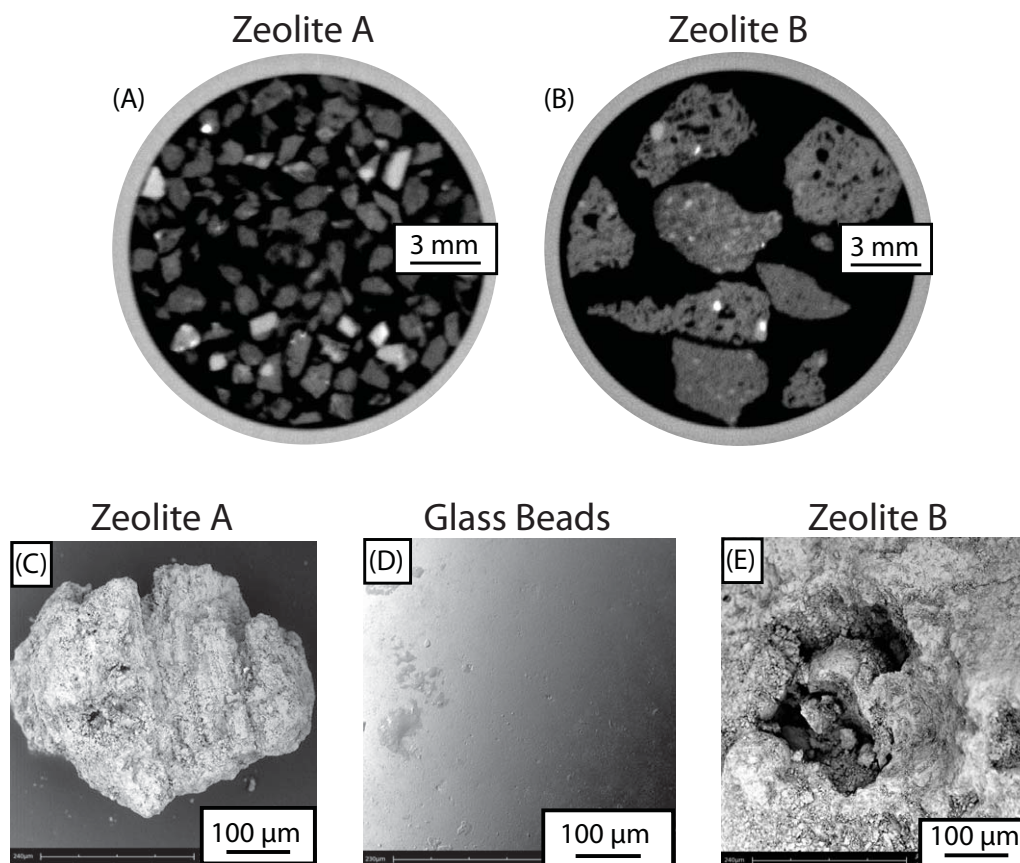
Figure 1. The materials used varied in size and composition. The synthetic glass beads were used as a reference, and two zeolites were sieved to five different sizes. CT (a, b) and SEM (c–e) images show the different intragranular pore structures between the two zeolites and the lack of intragranular pore structures in the glass beads. CT scans include all of the sieved fractions. Additional CT scans presented as a 3-D volume are included in the supporting information. Zeolite B has large intragranular pores throughout the entire grain that have a low degree of connectivity, and zeolite A has a more diffuse pore distribution.

different porous structures. The zeolites were individually sieved to differentiate the effects on mass transfer due to grain size and origin; different intragranular pore structures and pore volumes could lead to different θ_m, θ_{lm}, θ_{dc}, and α. Zeolite A was sieved to three different sizes (0.25–0.5 mm, 0.5–1 mm, and 1–2 mm), and zeolite B was sieved to two sizes (2–3.35 mm and 3.35–4.8 mm). We used synthetic 1.5 mm diameter glass beads with no internal porosity as a reference material (Figure 1).

3.1. Material Characterization
We conducted measurements of standard material characterization to link the porosity structure to properties controlling the observed transport behavior. Separate measurements were collected on unsieved samples of zeolite A and B. Hg porosimetry (Micromeritics Autopore IV 9500) was used to determine the pore-size distributions. CT scans were performed on dry zeolite samples placed in a 15 mm diameter plastic tube, and measurements were made with an X-TEK Benchtop CT160Xi scanner at 60 keV at approximately 340 μA, with 1567 images obtained around the center of rotation. Images were reconstructed using X-TEK reconstruction software producing a 3-D image with a resolution of approximately 15 μm (Figure 1 and supporting information). SEM images were obtained using a Phenom Desktop SEM (Phenom World, Eindhoven, The Netherlands) with a resolution of 30 nm (Figure 1) for both the glass beads and the zeolites. All samples prepared for SEM were sputter coated with a layer of gold nanoparticles prior to analysis to alleviate sample charging.

3.2. Laboratory Experiments: Solute Tracer Tests
We used 13 cm long and 3 cm diameter columns with an unpacked volume of 92 cm^3 for solute tracer tests (Figure 2). The columns were wet-packed, adding small amounts of material to a degassed water-filled
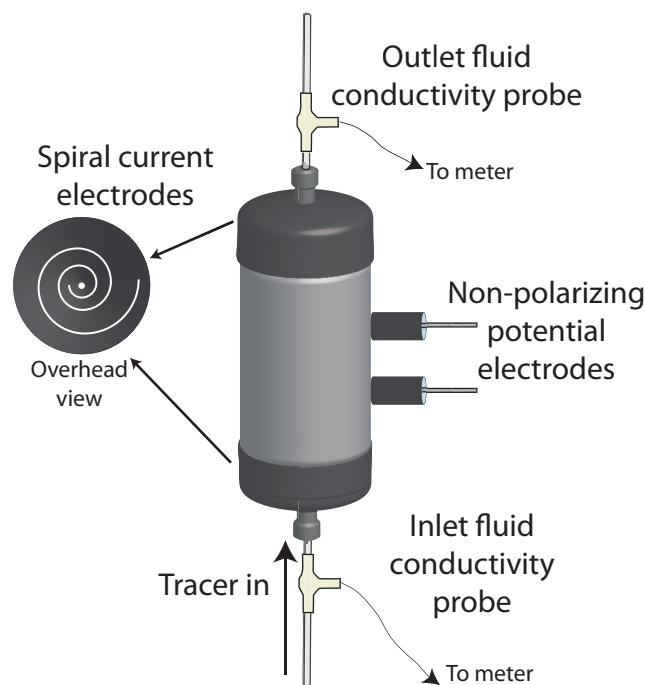
Figure 2. Solutes were injected into the base of the column, and σ_f was monitored at the bottom and the top of the column. Spiral current electrodes were at the top and bottom of the column, and two nonpolarizing electrodes were used to measure the potential difference. Syringe pumps (not pictured) were used to control the flow rate. DC and CC measurements were collected before and after tracer tests; NMR and material characterization were completed on samples packed in separate sample holders.

column, followed by tapping on the sides and the top of the material for complete compaction. No air bubbles were visible in the columns. Solute tracer tests were conducted for each of the five sieved fractions of zeolites and for the glass beads. A 0.4 g L^{-1} ($\sigma_f \sim$ 80 mS m^{-1}) background NaCl solution was injected into the bottom of each column at a rate of 0.35 mL min^{-1} until the solution reached equilibrium, determined by no change in σ_f, and steady state flow conditions were obtained. The time to reach equilibrium is controlled by α, which was not known before calibration to a transport model although we expected to be associated with geophysical data, explained earlier. After steady state was achieved, the injection line was switched to a continuous 0.35 mL min^{-1} stream of 1.15 g L^{-1} ($\sigma_f \sim$ 230 mS m^{-1}) NaCl tracer solution. Syringe pumps were used to inject the NaCl solution at a constant flow rate that was verified with volumetric checks of the column effluent. Every 30 s, σ_f was measured at both the inlet and outlet of the column using a flow-through σ_f electrode (Microelectrodes, Inc.).

We assumed that the NaCl solution is chemically conservative and that there is no retardation from sorption; therefore, any anomalous transport of the NaCl is attributed to physical heterogeneities, including diffusion into and out of θ_{lm}. This assumption must be taken with caution when applied to the zeolite, although clinoptilolite is preferentially selective toward Ca^{2+} over the tracer cation, Na$^+$ [*Hulbert*, 1987]. Retardation due to sorption would delay the tracer arrival and result in a greater estimated θ_m [*Singha et al.*, 2011].

3.3. NMR Measurements

Samples were prepared for NMR measurements by separate packing into Teflon containers using the same methods as described in *Swanson et al.* [2012]. After packing, the sample holders were vacuum-saturated in a 0.01 mM NaCl solution as described in *Keating and Knight* [2010]. Following saturation, the zeolite-packed sample holder was left submerged in the saturating fluid for one week, after which we assumed equilibrium had been reached and the sample was fully saturated. Prior to NMR measurements, the sample holders were covered with Parafilm to prevent evaporation.

NMR relaxation data were collected with a 2 MHz Rock Core Analyzer (Magritek Ltd) using a CPMG (Carr-Purcell-Meiboom-Gill) pulse sequence. Forty data points were obtained at each echo in the CPMG pulse sequence. Data were collected at an echo time of 200 μs; 50,000 echoes were collected for a total scan time of 10 s. The data were stacked 32 times such that the signal-to-noise ratio was greater than 200 for each measurement. A relaxation delay time of 10 s was used for each measurement to ensure that the samples returned to thermal equilibrium between each scan. The measurements were repeated in triplicate and all measurements were collected at the standard operating temperature of the instrument (30°C).

The relaxation time distribution for each NMR data set was determined using a nonnegative least-squares inversion with Tikhonov regularization as described by *Whittall et al.* [1991]. NMR data sets with more than

Sieved fraction [mm]		Zeolite A			Zeolite B		Glass beads
		0.25 to 0.5	0.5 to 1	1 to 2	2 to 3.35	3.35 to 4.8	1.5
Transport	Log$_{10}$ a (s^{-1})	-3.8	-3.6	-3.8	-3.5	-3.5	-3.3
	θ_m [-]	0.57	0.56	0.58	0.49	0.49	0.38
	θ_{lm} [-]	0.03	0.05	0.04	0.06	0.06	0.02
	$\theta_m + \theta_{lm}$ [-]	0.60	0.61	0.62	0.55	0.55	0.40
	Gravimetric θ [-]	0.69	0.68	0.68	0.64	0.64	0.42
	NMR Total θ [-]	0.62	0.63	0.64	0.62	0.63	0.41
DC Resistivity	σ_s [mS m^{-1}]	11	12	10	12	10	0.2
	F [-]	2.8	2.9	2.7	3.7	3.4	3.9
	m [-]	2.8	2.8	2.6	2.9	2.7	1.6
	τ [-]	1.9	2.0	1.8	2.4	2.2	1.7
	G [-]	0.36	0.34	0.37	0.27	0.29	0.26

Figure 3. The transport, NMR, and DC results. The blue and red entries correspond to θ_m and θ_{lm} estimates, respectively. The entries with a gray background correspond to all of the porosity estimates.

5000 data points were logarithmically subsampled to 5000 data points to improve the speed of the fitting algorithm. The subsampled data were then fit to a distribution of 160 exponentially spaced T_2-values ranging from 0.1 ms to 10 s. For each data set, the regularization parameter was selected using the L-curve criterion.

3.4. DC Resistivity Measurements
DC resistivity measurements were performed using a high-accuracy electrical impedance spectrometer described in *Zimmermann et al.* [2008]. Two nonpolarizing 0.8 mm Ag-AgCl potential electrodes were placed at the sides of the column at 4.5 and 8.5 cm from the base of the packed sample. Two stainless-steel current electrodes were installed in spiral configurations (see Figure 2) at the ends of both columns separated by 17 cm, with a 2 cm gap between the packed material and the current electrodes filled by a plastic porous disc. The porous disc dispersed the fluid flow evenly across the column end cap and prevented the porous material from escaping out of the column. We measured σ_b of the saturated, packed column at seven different σ_f (approximately 70, 110, 155, 200, 530, 1000, and 1600 mS m^{-1}). Measurements were collected at steady state flow conditions and equilibrium concentrations.

3.5. CC Measurements
CC measurements were collected using the same nonpolarizing potential electrodes as the DC resistivity measurements outlined in the previous section. Measurements were made at 23 injected frequencies in the range from 2 mHz to 14 kHz and were collected before ($\sigma_f \sim 80$ mS m^{-1}) and after ($\sigma_f \sim 230$ mS m^{-1}) tracer tests. Triplicate spectra were obtained and the average spectra were modeled using the Debye decomposition approach of *Keery et al.* [2012] to determine a bimodal distribution of CC relaxation times.

4. Results
Below, we present the results of the material characterization methods. Then, we analyze the tracer test and estimated DDMT parameters. Next, we present the DC, CC, and NMR measurements, and we use these data to partition the pore structure into θ_m, θ_{lm}, and θ_{dc} for comparison with values estimated with our tracer tests.

4.1. Material Characterization
CT (Figures 1a and 1b) and SEM (Figures 1c–1e) images of both zeolites reveal a notable intragranular porosity component. SEM images reveal no intragranular pore space component in the glass beads. Gravimetric porosity measurements for zeolites A and B are similar (0.64–0.68, Figure 3). The largest openings to a pore revealed from Hg porosimetry are shown in Figure 4 for unsieved samples of zeolite A and B. Zeolite
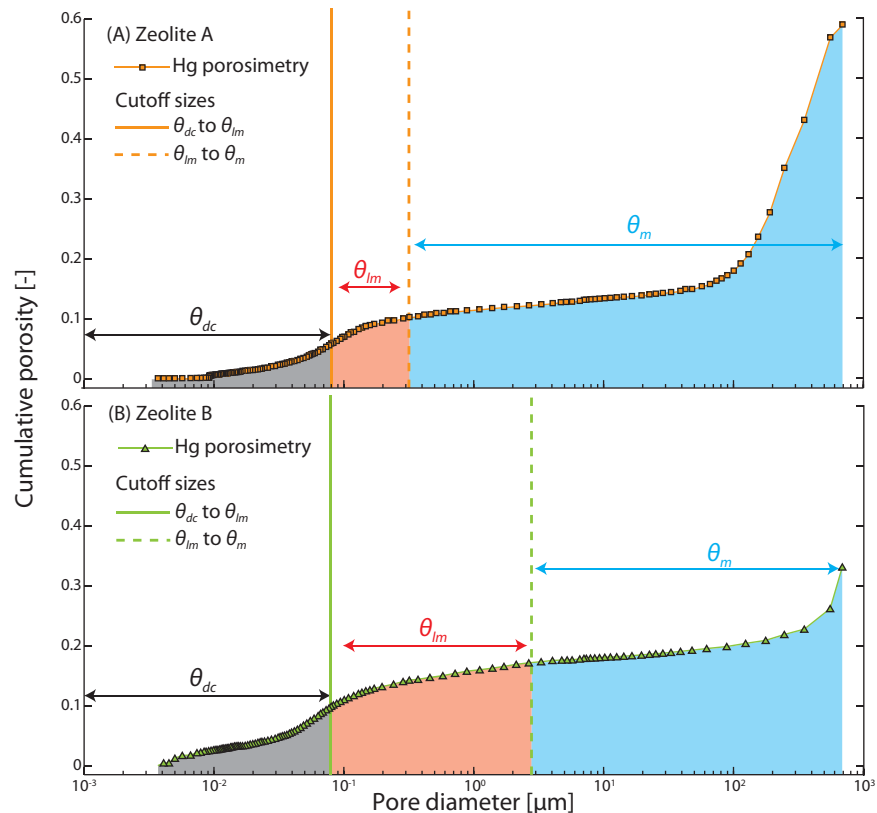
Figure 4. The results of the Hg porosimetry data show the cumulative porosity distribution from approximately 0.01 up to 700 μm for unsieved samples of zeolites A and B. The average difference between the transport and gravimetric porosity for the two zeolites, θ_{dc}, is not active for transport. Cutoff values for θ_m and θ_{lm} are based on model calibration and assume that pores of a similar size have the same surrounding pore environment including degree of connectedness. Zeolite A has a wider range of pore-sizes that act as θ_m.

A has a more continuous distribution of pore sizes compared to zeolite B. The lower limit and upper resolution limits are approximately 0.03 and 700 μm, respectively. We assume pore sizes larger than the upper limit correspond with θ_m [*Nimmo*, 2004], and some larger pores in zeolite B are likely not captured.

4.2. Tracer Tests and Solute Behavior

We use the parameter estimation software PEST [*Doherty*, 2010] to estimate the dispersivity and the single-rate DDMT parameters (θ_m, θ_{lm}, and the single α) using STAMMT-L (Figure 3). The 95% confidence intervals from PEST are within 1% for all porosity values. The estimated dispersivity ranged from 1.5 to 4.7 mm. The best-fit simulated BTCs are shown next to the observations in Figure 5. The advection timescale is inversely proportional to θ_m, so faster arrival times indicate a smaller θ_m. The mean arrival time is strongly controlled by θ_m so our analysis has greater sensitivity to this parameter [*Ciriello et al.*, 2013] than θ_{lm}.

Both zeolites have similar θ_m and θ_{lm} across all sieved fractions, and have some θ_{dc}, determined by the difference in transport-estimated and gravimetric porosity (Figure 3). Zeolite B has a smaller θ_m, greater θ_{lm}, and larger α compared to zeolite A (e.g., Figure 4). The estimates of θ_m, θ_{lm}, and α indicate no significant trends of DDMT parameters within the subfractions of each zeolite. Zeolite A has a longer residence time than zeolite B because α is inversely proportional to the residence time of solutes within θ_{lm} [*Haggerty et al.*, 2000]. The glass beads show negligible mass transfer.

4.3. NMR

The NMR relaxation time distributions differ substantially from sample to sample (Figure 6). The NMR relaxation time distribution for the glass beads is dominated by a large peak at long relaxation time that is assumed to correspond to intergranular pore water, and there is little response at shorter NMR relaxation times. This NMR response does not indicate intragranular porosity in the glass beads, which is consistent
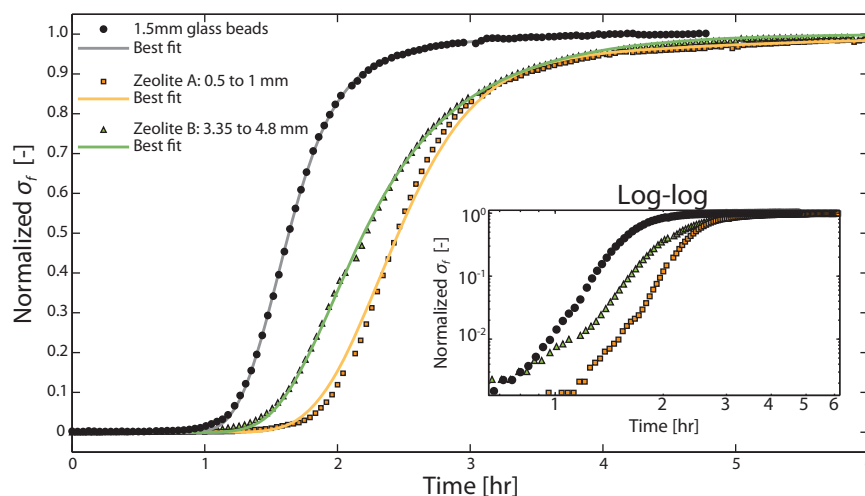
Figure 5. Best-fit simulations (solid lines) and observations (symbols) for the glass beads and one of each of the zeolite subfractions, with a subset showing the response in log-log space. The three different materials used have different BTC responses, indicating different mass transfer properties. The sieved subfractions for each zeolite have a similar BTC, so only a representative BTC is shown for σ_f every 150 s. Early arrival is indicative of a smaller θ_m. The effect of mass transfer appears in the two zeolites as tailing and the gradual increase in normalized σ_f until the input σ_f is reached.

with observations of the grain surface from SEM images. Conversely, for zeolite A and zeolite B, relaxation occurs with both long and short relaxation times. Zeolite A has a more continuous distribution of NMR relaxation times than zeolite B, which exhibits multiple discrete, isolated peaks.

The optimal NMR cutoff times that match the estimated θ_m and θ_{lm} (Figure 6) are determined by assuming the largest relaxation times and pores are θ_m, then assuming shorter times are θ_{lm} and finally assuming the rest of the signal corresponds to θ_{dc}. These estimated cutoff times are approximately 3 ms in zeolite A, but are approximately 1.5 s in zeolite B.

The glass beads and zeolites both show that the dominant response is controlled by intergranular pore space at long relaxation times (Figure 6). However, at faster relaxation times (around 10^{-3} s and associated with smaller pores), the glass beads have little response but there is a strong signal response in particular for zeolite B (Figure 6).

4.4. DC Resistivity
We measured σ_b at various σ_f (Figure 7) to estimate the formation factor F (the inverse of electrical connectedness G) and σ_s, respectively (equation (6); Figure 3). G is greater in zeolite A (0.34–0.37) compared to zeolite B (0.27–0.29), indicating greater electrical connectivity (equation (10)), likely as a function of decreased electrical tortuosity since the total porosity is similar for the two zeolites.

4.5. Complex Conductivity
CC measurements reveal peak polarization (expressed here as chargeability) increases with relaxation time for the zeolites (Figure 8). There is a distinct peak in the CC relaxation time distribution for the two finest sub-fractions of zeolite A, and the peak CC relaxation time is associated with increased grain size, independent of zeolite A or B, consistent with equation (11). Independent of grain size, the response is greater for zeolite A than zeolite B.

5. Discussion

We collected measurements of porous media using material characterization methods and tracer experiments, and built upon these standard techniques by considering also static NMR, DC resistivity, and CC measurements. We seek to interpret the geophysical measurements in terms of DDMT parameters needed for predictive modeling. A summary of the results are shown in Table 1 and Figure 9, which relates the transport, geophysical, and material characterization methods used here.
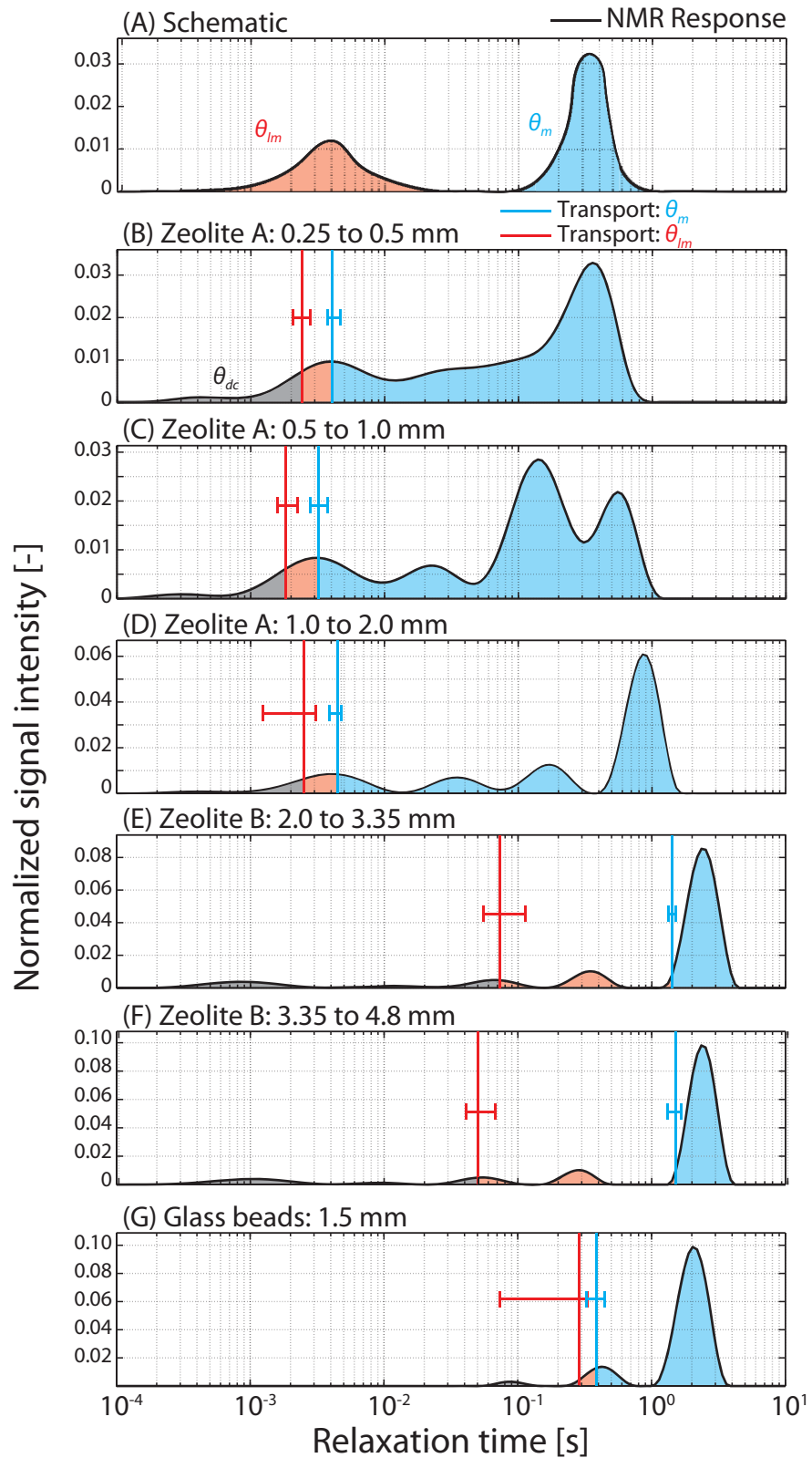
Figure 6. (a) The schematic shows an idealized NMR relaxation time distribution dominated by two distinct peaks that would correspond to θ_m or θ_{lm}, given by a single cutoff time. In the subsequent subplots (b–g), the NMR relaxation time is shown for each of the samples. The transport-estimated best fit θ_m and θ_{lm} are shown as blue and red lines, respectively, with associated error bars assuming a 1% error in the estimated θ_m and θ_{lm}.
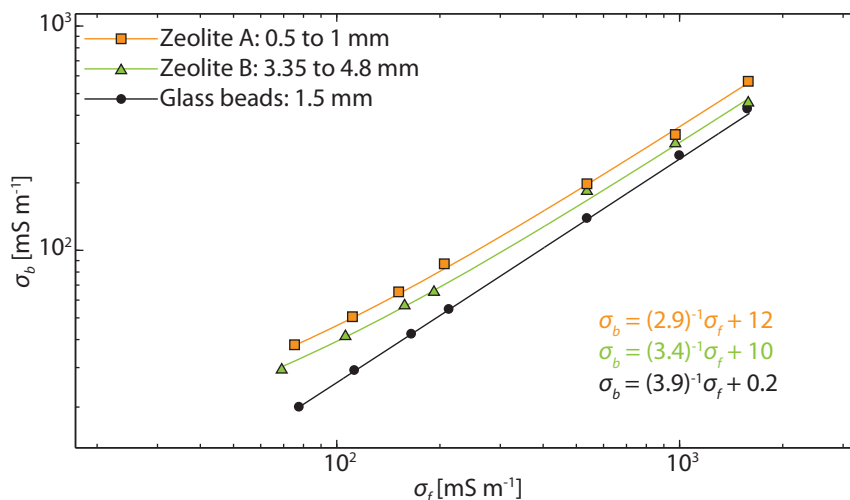
Figure 7. The measured σ_b and σ_f for the glass beads and a representative sample of the two zeolites, and a best fit of equation (6) for each.

5.1. Model Calibration of DDMT Parameters

Tracer tests on both zeolites exhibit non-Fickian BTCs that could not be fit using the ADE. Zeolite A and B were sieved to identify possible relation between grain size and DDMT parameters. Differences in transport behavior were driven by differences in pore structure and independent of grain size. Any substantial differences in estimated DDMT parameters between zeolite A and B are attributed to the unique intragranular pore structure of the two zeolites given their different origins and thus pore structure, rather than grain size (Figure 3). The PEST estimates of θ_{lm} (0.02) and α (5×10^{-4} s^{-1}) for the glass beads indicate little DDMT. Minor mass transfer may be the result of possible dead-end pore space due to packing arrangements [*Scheibe et al.*, 2013]; however, it should be noted that non-zero θ_{lm} and α may yet be consistent with negligible mass transfer. For a given experimental setup (flow rate and experiment duration), various combinations of parameters would not produce observable mass transfer. The simple addition of more parameters (α and θ_{lm}) in the DDMT model compared to the ADE model may provide a superior fit to data but may not indicate substantial mass transfer.

We used the linear approximation for parameter estimation in PEST and estimated transport parameters for a single-rate DDMT model for simplicity. However, the complex pore structure of the zeolite may require a more complex transport model such as the MRMT model. Repeating the experiment at flow rates orders of magnitude faster and slower would result in different flow conditions that may reveal MRMT behavior, but repeating the experiments at different flow rates poses additional challenges. At faster flow rates, the temporal resolution of σ_f measurements may not be sufficient and the full effect of tailing may not be captured. At slower rates, the tailing and experimental duration are prolonged, and the effects of possible instrumentation drift in the σ_f signal are magnified, reducing the resolution of the captured tail of the BTC. A stochastic approach may result in different estimated single-rate DDMT parameters from the BTCs, but these estimated parameters are not necessarily more representative of the physical description of the pore structure of the zeolites for a single-rate DDMT model. As a result, we focus less on applying our geophysical methods to provide parameter estimation, and focus more on integrating these geophysical methods as diagnostic tools to analyze the pore environment.

The total gravimetric porosity is similar for the two zeolites, but CT scans show that zeolite A lacks the large, isolated pores observed in zeolite B. The lack of the large pores but similar porosity suggests that the intragranular pore network in zeolite A is more well-connected compared to zeolite B because the pores must be smaller and distributed throughout the grains in zeolite A. This is consistent with the greater G and NMR relaxation time distributions in zeolite A (0.34–0.37 for G) compared to zeolite B (0.27–0.29 for G).

For both zeolites, the total porosities (0.60–0.62 for zeolite A, 0.55 for zeolite B) estimated from the tracer tests are smaller than measured gravimetric porosities (0.68–0.69 for zeolite A, 0.64 for zeolite B), indicating
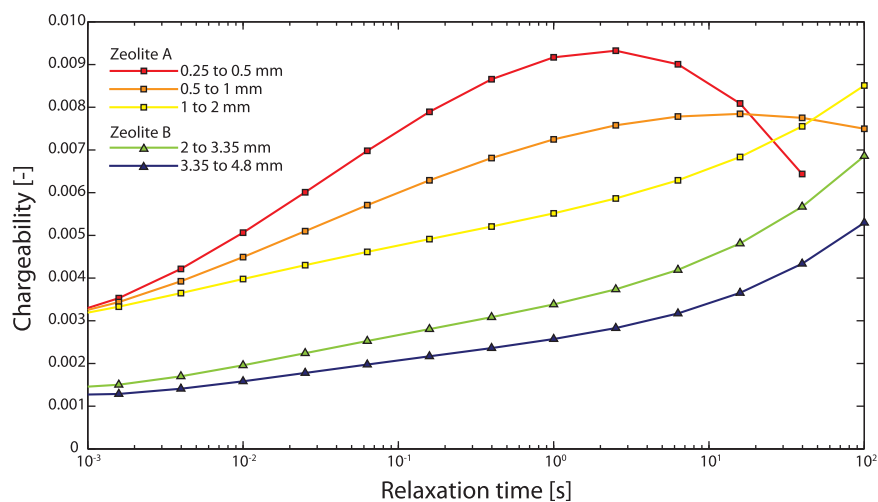
Figure 8. The CC spectra from Debye decomposition. The response at larger CC relaxation times is controlled by grain size, whereas the response at smaller CC relaxation times corresponds to a difference in the pore structures. There is a distinct difference between the two zeolites for the smaller CC relaxation time distributions.

that some of the porosity may not be active for transport. The difference between gravimetric porosity and total estimated porosity ($\theta_{lm}+\theta_m$) is similar for zeolite B (0.09) than zeolite A (0.06–0.09). This apparent discrepancy has two explanations: (1) there is physically disconnected porosity not available for transport, or (2) the rate of solute exchange is so slow relative to advection that there is not sufficient time for mass transfer into some of the pore space, corresponding with $DaI \ll 1$. Hg porosimetry and NMR may be sensitive to pore space that is not captured with our model calibrations. Hg porosimetry is conducted at much higher pressures than our laboratory experiments and therefore may be exposed to active pore space that may be otherwise immobile during our tracer experiments. NMR may be sensitive to pore space that is untouched by solutes in our experiment. Here, we attribute the porosity difference to θ_{dc}, with the understanding that the effective θ_{dc} may be different for different experimental conditions.

We estimate the pore size for θ_{dc} is approximately 0.08 µm for both the zeolites based on the pore size estimates from Hg porosimetry (Figure 4). These small pores may not actively contribute to advective transport or solute exchange. The pore-size threshold that separates θ_{lm} and θ_m (determined by the sum of θ_{lm} and θ_{dc}) corresponds with pores greater than 0.3 µm and 3 µm for zeolite A and B, respectively (see Figure 4). θ_{lm} in zeolite B consists of larger pores and spans a wider pore-size distribution than zeolite A. The 0.3–3 µm pore-size range that is θ_m in zeolite A is θ_{lm} in zeolite B. These delineations of Hg porosimetry pore sizes for each zeolite from our calibrations of BTCs into θ_{dc}, θ_{lm}, and θ_m are based upon the assumption that any given pore size will have identical transport properties, which may not be the case. Rather than use this assumption to split the porosities in a quantitative way, we focus primarily on descriptive information derived from Hg porosimetry measurements, such as the relative differences in pore sizes between zeolite A and B (Table 1).

We note that other models of nonlocal solute transport may have physical connections to the pore properties of the media besides DDMT, including the spherical-diffusion model (SDM) [*Goltz and Roberts*, 1986], which also was evaluated for this work (see Appendix A). Similar to the DDMT model, the SDM tracks two concentrations: (1) the concentration in a mobile pore space, and (2) the concentration in the intragranular pore space. One potential advantage of the SDM includes the ability to reproduce BTC behavior for varying L and v, and thus, different flow conditions [*Young and Ball*, 1995] whereas the single-rate DDMT model may work effectively only for a range of DaI. Despite its intuitive appeal, the SDM does not provide a good fit to the transport behavior of the zeolites studied here. Whereas the SDM assumes that intragranular porosity is entirely immobile, a portion of the zeolite's intragranular porosity appears to behave as mobile porosity for advection. We note that the SDM and the MRMT model (and other models non-Fickian transport) may prove advantageous for work on other materials.

Table 1. A Summary of the Conclusions Drawn From the Methods Used

Method	Zeolite A	Zeolite B
CT scans	Small pores throughout the grains	Large pores isolated in the grains
Hg porosimetry	Smaller pores than zeolite B	Larger pores than zeolite A, largest pores are missed
Gravimetric porosity	Slightly larger than zeolite B	Smaller than zeolite A
NMR	Continuous distribution, multimodal peaks	Discrete distribution, few isolated peaks
G (connectedness)	Larger than zeolite B	Smaller than zeolite A
Tortuosity	Smaller than zeolite B	Larger than zeolite A
Complex conductivity	Larger response at shorter relaxation times	Larger response at longer relaxation times
	Peak chargeability at shorter relaxation times	Peak chargeability at longer relaxation times
Tracer test	Larger mobile porosity than zeolite B	Slightly larger less-mobile porosity than zeolite A
	Total estimated porosity is less than gravimetric	Total estimated porosity is less than gravimetric
Conclusions from these data		

1. Zeolite A has smaller pores but a larger porosity than Zeolite B, and that pore space is better connected and less tortuous than Zeolite B.

2. Zeolite B has larger pores and a smaller porosity than Zeolite A, and that pore space is less well-connected and more tortuous than Zeolite B.

3. Both zeolites have a component of porosity (1) in which advection occurs, (2) diffusive exchange occurs, and (3) that is disconnected from transport but still present.

5.2. Nuclear Magnetic Resonance

The shape of the NMR relaxation time distributions (Figure 6) implies that zeolite A has a more continuous pore-size distribution compared to zeolite B. The NMR-estimated and gravimetric porosity are greater than the transport total porosity, indicating a θ_{dc} component. A single NMR cutoff time may not effectively discriminate between θ_m and θ_{lm} because the cutoff values are likely flow-rate dependent and may vary with the connectedness of the pore structures, which are material dependent. Another cutoff time may be needed to account for the saturated θ_{dc} that does not contribute to transport but is sensitive to NMR and
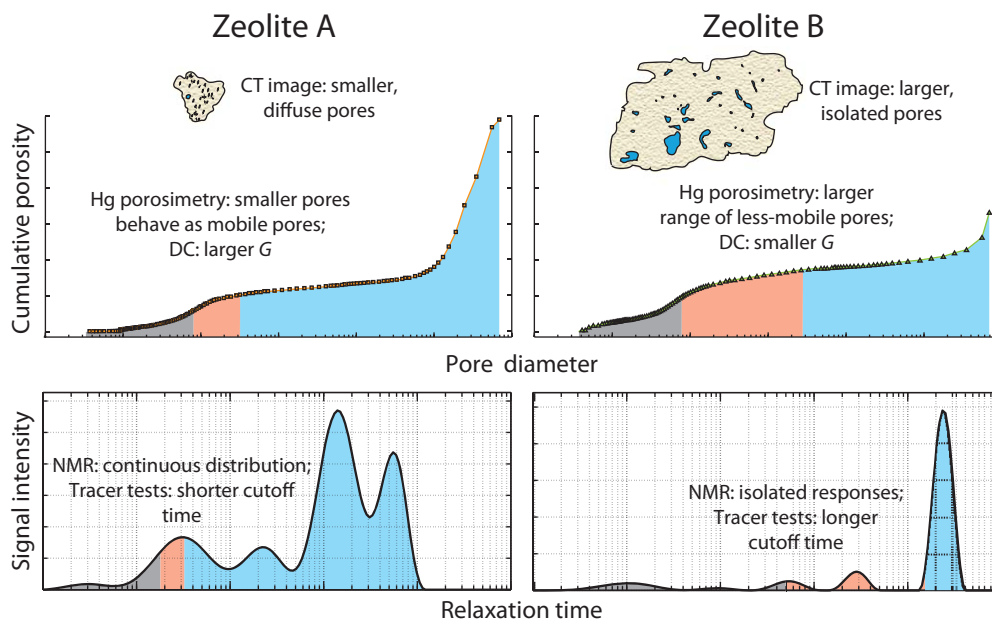

Figure 9. A simplified summary of the contrast in properties between zeolite A and zeolite B. Zeolite A has smaller and more continuous distribution of pores along with a larger G; zeolite B has larger, isolated pores and a smaller G. The gray, red, and blue correspond to θ_{dc}, θ_{lm}, and θ_m, respectively.

SWANSON ET AL.   1277

gravimetric measurements. Although the cutoff time for θ_{dc} may change between samples, the cutoff time may be controlled by a minimum pore-size if we assume θ_{dc} corresponds to the smallest pores, and this volume and threshold can be measured through Hg porosimetry.

Small pores at the conjunction of grains will be captured with NMR, but these small pores are connected to larger intergranular pores. Consequently, relaxing protons diffuse through the pores and average over the entire connected pore space and the pore throat appears similar to that of the larger pore as a whole and is interpreted as θ_m. This is in contrast to small, disconnected intragranular pores that are not well-connected to the rest of the connected pore network and are interpreted as θ_{lm}. If the largest peak of the NMR relaxation time distribution encompasses all of the intergranular porosity (Figure 6), then some of the intragranular porosity must be active for advection according to tracer tests, and thus part of θ_m.

The NMR relaxation time distribution is more multimodal in zeolite B than A, and thus slight changes in the assumed cutoff time will not substantially change the estimated θ_m and θ_{lm} for zeolite B. Conversely, zeolite A has a more continuous distribution than zeolite B, and estimates of θ_m and θ_{lm} are more sensitive to the selected cutoff time. NMR estimates of bound and producible pore volumes provide limited insight for predicting transport behavior; the NMR relaxation time distribution is not easily separated into θ_m and θ_{lm} necessary for DDMT models. One issue is that NMR is not sensitive to the connectivity of the pores, so large, disconnected pores could be interpreted as θ_m and small well-connected pores active for advection could be interpreted as θ_{lm}.

5.3. DC Resistivity

DC resistivity can provide indicators of the connectedness, *G*, of the porous media, and a continuous pore-size distribution may be associated with greater values of *G*. We assume that θ_{dc} contributes to the measurement of *G* given that it is a part of θ_{tot}, and that the electrical connectivity is related to and systematically larger than the transport connectivity [*Zhang and Knackstedt*, 1995]. Equation (10) shows that *G* varies linearly with θ_{tot}, which includes θ_{dc}. Regardless of whether θ_{dc} contributes to *G*, the relative size of *G* of zeolite A to zeolite B would remain the same such that zeolite A would be described as more connected than zeolite B according to these data. *G* is greatest for zeolite A, indicating a higher potential for connected pathways between more and less-mobile domains (Figure 3). We argue that smaller pores in zeolite A advect solutes, whereas those of zeolite B do not because: (1) based on our calibrated porosities from tracer test BTCs, the Hg porosimetry indicates a more continuous distribution for zeolite A compared to B (Figure 4), and (2) *G* is greater in zeolite A (0.34–0.37) than zeolite B (0.27–0.29) and the increased connectivity is associated with additional, smaller mobile pores (Figure 8).

The Hg porosimetry data reveal that zeolite A has smaller pores, and DC resistivity indicates a greater value of *G* in zeolite A (0.34–0.37), compared to zeolite B (0.27–0.29). There does not appear to be a distinct pore size that separates θ_m or θ_{lm}; rather, the transport properties of a given pore depend on the material surroundings and the degree of connectedness to the rest of pore volume. NMR cutoff time discriminates bound and unbound pores based on pore size rather than a measure of connectivity, the latter of which is critical to mass-transfer processes. While the NMR cutoffs between mobile and immobile porosity do not make sense given the relaxation time distributions, we do notice the following pattern in homogenous systems: smaller *G* (i.e., poorer connectivity) may be associated with larger predicted NMR relaxation time cutoffs between mobile and immobile porosity. In the presence of low connectivity, a larger cutoff time may be needed because some large pores may be isolated and contribute to θ_{lm}. Conversely, in the presence of strong connectivity, a shorter cutoff time may be needed to assign more pores to θ_m.

5.4. Complex Conductivity

CC relaxation times show peak chargeability associated with increasing grain size, consistent with equation (11). If the peak chargeability response is controlled by grain size [*Schwarz*, 1962], consistent with these observations, then the faster CC relaxation times correspond with a shorter length scale and must be due to (possibly intragranular) subgrain-scale polarization mechanisms. Zeolite A has a greater contribution to total polarization from shorter length scales than zeolite B (Figure 8). However, there is no clear trend between CC relaxation time and α. Consequently, we conclude a null hypothesis given our expectations: the length scales of intragranular electrical polarization do not appear to be directly related to length scales of diffusive

mass transfer. CC measurements are likely sensitive to the grain size, which may have other applications for transport characterization outside of the DDMT model.

6. Conclusions

Geophysical measurements indicate that pore connectivity is important for transport processes and pore-size distribution is insufficient for evaluating rate-limited mass-transfer effects on transport. We presented column-scale tracer tests, material characterization, and geophysical data collected on two zeolites and a glass-bead reference to explore relations between intragranular pore structures and parameters driving anomalous, non-Fickian solute transport in saturated porous media. Through model calibration, we estimate different θ_m and θ_{lm} for the two different zeolites. Tracer tests and model calibration on sieved fractions of the zeolites indicate that the best-fit DDMT parameters are not controlled by grain size.

We show that DC resistivity measurements may be useful for describing the connectedness of the pore structure. Zeolite A has a shorter NMR relaxation time cutoff based on transport estimates of θ_m and θ_{lm} (Figure 6). In this zeolite, Hg porosimetry reveals that smaller pores contribute to advective transport (Figure 4). We propose that the internal porous network of zeolite A is more continuous with smaller pores because the NMR relaxation time distribution is more continuous (Figure 6) and G is larger (Figure 3); however, this conclusion may a consequence of the selection of inversion parameters for the NMR data set. Increased pore space active for advective transport shifts the cutoff towards smaller NMR relaxation times because the NMR relaxation time distribution is controlled by pore-size distributions. The internal pores are relatively large and more isolated in zeolite B than in zeolite A as shown in the CT images and the 3D videos (see supporting information), which correspond with NMR relaxation times dominated by a large intragranular response at longer times and isolated smaller intragranular responses at shorter NMR relaxation times. Our results can be summarized in the following major conclusions:

1. We provide the first laboratory experiments interpreting NMR relaxation time distributions for DDMT models, and find that NMR provides approximate pore size distributions; however, directly constraining mobile and less-mobile porosities in terms of transport from these distributions remains elusive. This is complicated by the fact that optimal cutoff times to partition mobile/less-mobile porosity are dependent on the material and flow rate. For these samples, NMR is unable to separate mobile and less-mobile porosities required for DDMT systems.

2. The DC-resistivity derived estimates of G are indicative of transport connectivity and thus θ_m. Through analysis of the pore sizes from Hg porosimetry, NMR relaxation time distributions, and tracer tests, we find that increasing pore connectivity is associated with in smaller pores advecting solutes, whereas a decrease in the connectivity is associated with more pores behaving as θ_{lm}. Pores may be either mobile or less-mobile depending on their surroundings; pore sizes that are considered mobile may be less-mobile within the same or across different materials.

3. CC measurements do not appear to be related to α and thus are not associated with the residence times within θ_m. At larger CC relaxation times, the polarization response is dominated by grain size. At shorter CC relaxation times, there is a substantial difference between the polarization response between the zeolites that cannot be attributed to a grain size effect alone. Relations between these observations and our transport observations were unclear. CC is primarily related to surface rather than pore characteristics; consequently, CC may be dominated by other hydrogeologic parameters not related to DDMT [see, e.g., *Slater*, 2007].

The extension of our results to field experiments is subject to complications including possible low-permeability zones that behave similarly to θ_{lm}, heterogeneities of K, θ, σ_b, and σ_f, and mineral composition. However, field-scale measurements of σ_b can be used to estimate G to determine different zones of high and low connectivity and potential regions for mass transfer. The static geophysical approaches discussed here (NMR, DC resistivity) may be better suited as diagnostic tools for evaluating transport process, rather than noninvasive measurements for predicting transport properties. However, these static geophysical methods provide additional information related to the pore structure and serve as additional information to traditional characterization methods such as tracer tests and measurements of K. A combination of these measurements with time-lapse electrical monitoring of tracer experiments [e.g., *Day-Lewis and Singha*,

2008; *Briggs et al.*, 2013, 2014] may allow for more effective and cost-effective characterization of field-scale DDMT parameters.

The aim of this paper was to provide experimental methods, results, and observations for measuring and characterizing the pore structure of porous media that may drive non-Fickian transport that cannot be described by ADE-based models of solute transport. Based on our results, NMR and DC resistivity measurements have potential as diagnostic tools to describe features of the pore structure that may drive tailing. These geophysical methods may have limited ability to predict transport properties directly, but can be used at the lab and potentially field scale to describe pore connectivity and size, which can be useful to evaluating properties of interest. CC measurements, however, appear to provide little information about DDMT parameters, at least for the zeolites considered. Our findings point to the potential and limitations of geophysical and material characterization methods to provide useful insight into the controlling factors of anomalous solute transport, and as diagnostic tools for evaluating transport processes.

Appendix A: Spherical-Diffusion Model (SDM)

We estimate the SDM model parameters using PEST, matching the flow conditions for the column experiments and using the median grain radii for each of the sieved fractions. The estimated porosities from the calibrated model exceeded the gravimetric porosity for both zeolites A and B, resulting in a nonphysical description of the pore space. The mobile and less mobile porosity for zeolite B (2–3.35 mm) was 0.43 and 0.82, respectively, and for zeolite A (0.5–1 mm) was 0.52 and 0.50, respectively. Whereas the SDM assumes that intragranular porosity is effectively immobile, advective transport likely occurs within a well-connected portion of the intragranular pore space of these zeolites. As a result, the SDM model does not adequately describe the primary mechanism for solute transport (advection) for the zeolites. Consequently, we focus exclusively on the DDMT model because geophysical measurements have been shown to be sensitive to solutes in θ_m for time-lapse monitoring [*Singha et al.*, 2007; *Swanson et al.*, 2012] but little work has been done exploring the relation of static geophysical measurements to DDMT parameters without subjecting the material to invasive tracer tests.

Notations

ADE	Advection-dispersion equation
DDMT	Dual-domain mass transfer
NMR	Nuclear magnetic resonance
DC	Direct-current (resistivity)
CC	Complex conductivity
BTC	Breakthrough curve
SEM	Scanning electron microscope
CT	X-ray computer tomography
MRMT	multirate mass transfer
DaI	Damköhler number
SDM	Spherical-diffusion model

Notation	Meaning	Units
a_i	Characteristic length scale	m
C_{lm}	Concentration in θ_m	kg m^3
C_m	Concentration in θ_{lm}	kg m^3
D	Dispersion coefficient	m^2 s^{-1}
$D*$	Diffusion coefficient	m^2 s^{-1}
F	Formation factor	(-)
G	Electrical connectedness	(-)
I_0	Normalized initial signal amplitude	(-)
K	Hydraulic conductivity	m s^{-1}

k	Geometric factor	m
L	Distance from observation to source of tracer solution injection	m
m	Cementation exponent	(-)
R	Resistance	Ω
R_g	Grain radius	m
t	Time	s
T_2	Transverse relaxation time	s
v	Average pore water velocity	m s^{-1}
x	Spatial coordinate	m
α	Mass-transfer rate coefficient	s^{-1}
α_L	Dispersivity	m
θ_{dc}	Disconnected porosity	(-)
θ_{eff}	Effective porosity	(-)
θ_{lm}	Less-mobile porosity	(-)
θ_m	Mobile porosity	(-)
θ_{TOT}	Total gravimetric porosity	(-)
ρ_{2i}	Surface relaxivity	m s^{-1}
ρ_b	Electrical resistance	Ω m
σ^*	Complex electrical conductivity	S m^{-1}
σ''	Imaginary conductivity component	S m^{-1}
σ_b	Bulk conductivity	S m^{-1}
σ_f	Fluid conductivity	S m^{-1}
σ_s	Surface conductivity	S m^{-1}
τ_r	Relaxation time	s
ζ	Electrical tortuosity	(-)

References

Allen, D., et al. (2000), Trends in NMR logging, *Oilfield Rev.*, *12*(2), 2–19.

Archie, G. E. (1942), The electrical resistivity log as an aid in determining some reservoir characteristics, *Trans. Am. Inst. Min. Metall. Pet. Eng.*, *146*, 54–62, doi:10.2307/777630.

Arns, C. H. (2004), A comparison of pore size distributions derived by NMR and X-ray-CT techniques, *Physica A*, *339*(1-2), 159–165, doi: 10.1016/j.physa.2004.03.033.

Bahr, J. M., and J. Rubin (1987), Direct comparison of kinetic and local equilibrium formulations for solute transport affected by surface reactions, *Water Resour. Res.*, *23*(3), 438–452, doi:10.1029/WR023i003p00438.

Benson, D. A., R. Schumer, M. M. Meerschaert, and S. W. Wheatcraft (2001), Fractional dispersion, Lévy motion, and the MADE tracer tests, *Transp. Porous Media*, *42*(1-2), 211–240.

Benson, D. A., M. M. Meerschaert, and J. Revielle (2013), Fractional calculus in hydrologic modeling: A numerical perspective, *Adv. Water Resour.*, *51*, 479–497, doi:10.1016/j.advwatres.2012.04.005.

Berkowitz, B., J. Klafter, R. Metzler, and H. Scher (2002), Physical pictures of transport in heterogeneous media: Advection-dispersion, random-walk, and fractional derivative formulations, *Water Resour. Res.*, *38*(10), 1191, doi:10.1029/2001WR001030.

Berkowitz, B., A. Cortis, M. Dentz, and H. Scher (2006), Modeling non-Fickian transport in geological formations as a continuous time random walk, *Rev. Geophys.*, *44*, RG2003, doi:10.1029/2005RG000178.

Bianchi, M., C. Zheng, G. R. Tick, and S. M. Gorelick (2011), Investigation of small-scale preferential flow with a forced-gradient tracer test, *Ground Water*, *49*(4), 503–14, doi:10.1111/j.1745-6584.2010.00746.x.

Binley, A., G. Cassiani, and R. Deiana (2010), Hydrogeophysics: Opportunities and challenges, *Bol. Geofis. Teor. Appl.*, *51*(4), 267–284.

Bird, N. R. A., A. R. Preston, E. W. Randall, W. R. Whalley, and A. P. Whitmore (2005), Measurement of the size distribution of water-filled pores at different matric potentials by stray field nuclear magnetic resonance, *Eur. J. Soil Sci.*, *56*(1), 135–143, doi:10.1111/j.1365-2389.2004.00658.x.

Bohling, G. C., G. Liu, S. J. Knobbe, E. C. Reboulet, D. W. Hyndman, P. Dietrich, and J. J. Butler Jr. (2012), Geostatistical analysis of centimeter-scale hydraulic conductivity variations at the MADE site, *Water Resour. Res.*, *48*, W02525, doi:10.1029/2011WR010791.

Börner, F. D., J. R. Schopper, and A. Weller (1996), Evaluation of transport and storage properties in the soil and groundwater zone from induced polarization measurements, *Geophys. Prospect.*, *44*(4), 583–601.

Briggs, M. A., F. D. Day-Lewis, J. B. T. Ong, G. P. Curtis, and J. W. Lane (2013), Simultaneous estimation of local-scale and flow path-scale dual-domain mass transfer parameters using geoelectrical monitoring, *Water Resour. Res.*, *49*, 5615–5630, doi:10.1002/wrcr.20397.

Briggs, M. A., F. D. Day-Lewis, J. B. Ong, J. W. Harvey, and J. W. Lane (2014), Dual-domain mass-transfer parameters from electrical hysteresis: Theory and analytical approach applied to laboratory, synthetic streambed, and groundwater experiments, *Water Resour. Res.*, *50*, 8281–8299, doi:10.1002/2014WR015880.

Brownstein, K. R., and C. E. Tarr (1979), Importance of classical diffusion in NMR studies of water in biological cells, *Phys. Rev. A*, *19*(6), 2446–2453.

Butler J. J. Jr., P. Dietrich, V. Wittig, and T. Christy (2007), Characterizing hydraulic conductivity with the direct-push permeameter, *Ground Water*, *45*(4), 409–419, doi:10.1111/j.1745-6584.2007.00300.x.

Ciriello, V., A. Guadagnini, V. Di Federico, Y. Edery, and B. Berkowitz (2013), Comparative analysis of formulations for conservative transport in porous media through sensitivity-based parameter calibration, *Water Resour. Res.*, *49*, 5206–5220, doi:10.1002/wrcr.20395.

Day-Lewis, F. D., and K. Singha (2008), Geoelectrical inference of mass transfer parameters using temporal moments, *Water Resour. Res.*, *44*, W05201, doi:10.1029/2007WR006750.

Dlubac, K., R. Knight, Y.-Q. Song, N. Bachman, B. Grau, J. Cannia, and J. Williams (2013), Use of NMR logging to obtain estimates of hydraulic conductivity in the High Plains aquifer, Nebraska, USA, *Water Resour. Res.*, *49*, 1871–1886, doi:10.1002/wrcr.20151.

Dogan, M., R. L. Van Dam, G. C. Bohling, J. J. Butler Jr., and D. W. Hyndman (2011), Hydrostratigraphic analysis of the MADE site with full-resolution GPR and direct-push hydraulic profiling, *Geophys. Res. Lett.*, *38*(6), L06405, doi:10.1029/2010GL046439.

Doherty, J. (2010), *PEST: Model-Independent Parameter Estimation*, 1–336, Watermark Comput. Corinda, Australia.

Ewing, R. P., C. Liu, and Q. Hu (2012), Modeling intragranular diffusion in low-connectivity granular media, *Water Resour. Res.*, *48*, W03518, doi:10.1029/2011WR011407.

Feehley, C. E., C. Zheng, and F. J. Molz (2000), A dual-domain mass transfer approach for modeling solute transport in heterogeneous aquifers: Application to the Macrodispersion Experiment (MADE) site, *Water Resour. Res.*, *36*(9), 2501–2515, doi:10.1029/2000WR900148.

Flach, G. P. (2012), Relationship between dual-domain parameters and practical characterization data, *Ground Water*, *50*(2), 216–29, doi:10.1111/j.1745-6584.2011.00834.x.

Giesche, H. (2006), Mercury porosimetry: A general (practical) overview, *Part. Part. Syst. Charact.*, *23*(1), 9–19, doi:10.1002/ppsc.200601009.

Glover, P. (2009), What is the cementation exponent? A new interpretation, *Lead. Edge*, 82–85.

Glover, P. W. J. (2010), A generalized Archie's law for n-phases, *Geophysics*, *75*(6), E247–E266.

Goltz, M., and P. V. Roberts (1986), Three-dimensional solutions for solute transport in an infinite medium with mobile and immobile zones, *Water Resour. Res.*, *22*(7), 1139–1148, doi:10.1029/WR022i007p01139.

Haggerty, R. (2009), *STAMMT-L version 3.0 User Manual*, Corvallis, Oregon State University, Oreg. [Available at http://www.science.oregon-state.edu/~haggertr/STAMMTL/.]

Haggerty, R., and S. M. Gorelick (1995), Multiple-rate mass transfer for modeling diffusion and surface reactions in media with pore-scale heterogeneity, *Water Resour. Res.*, *31*(10), 2383–2400, doi:10.1029/95WR01583.

Haggerty, R., S. A. McKenna, and L. C. Meigs (2000), On the late-time behavior of tracer test breakthrough curves, *Water Resour. Res.*, *36*(12), 3467–3479, doi:10.1029/2000WR900214.

Haggerty, R., C. F. Harvey, C. F. Von Schwerin, and L. C. Meigs (2004), What controls the apparent timescale of solute mass transfer in aquifers and soils? A comparison of experimental results, *Water Resour. Res.*, *40*, W01510, doi:10.1029/2002WR001716.

Harmon, T. C., and P. V Roberts (1994), Comparison of intraparticle sorption and desorption rates for a halogenated alkene in a sandy aquifer material, *Environ. Sci. Technol.*, *28*(9), 1650–1660, doi:10.1021/es00058a017.

Harvey, C. F., and S. M. Gorelick (2000), Rate-limited mass transfer or macrodispersion: Which dominates plume evolution at the Macrodispersion Experiment (MADE) site?, *Water Resour. Res.*, *36*(3), 637–650, doi:10.1029/1999WR900247.

Hinedi, Z. R., Z. J. Kabala, T. H. Skaggs, D. B. Borchardt, R. W. K. Lee, and A. C. Chang (1993), Probing soil and aquifer material porosity with nuclear magnetic resonance, *Water Resour. Res.*, *29*(12), 3861–3866, doi:10.1029/93WR02302.

Hulbert, M. H. (1987), Sodium, calcium, and ammonium exchange on clinoptilolite from the Fort Laclede Deposit, sweetwater county, Wyoming, *Clays Clay Miner.*, *35*(6), 458–462, doi:10.1346/CCMN.1987.0350606.

Keating, K., and S. Falzone (2013), Relating nuclear magnetic resonance relaxation time distributions to void-size distributions for unconsolidated sand packs, *Geophysics*, *78*(6), D461–D472.

Keating, K., and R. Knight (2010), A laboratory study of the effect of Fe (II)-bearing minerals on nuclear magnetic resonance (NMR) relaxation measurements, *Geophysics*, *75*(3), F71–F82, doi:10.1190/1.3386573.

Keery, J., A. Binley, A. Elshenawy, and J. Clifford (2012), Markov-chain Monte Carlo estimation of distributed Debye relaxations in spectral induced polarization, *Geophysics*, *77*(2), E159–E170, doi:10.1190/geo2011-0244.1.

Klein, J. D., and W. R. Sill (1982), Electrical properties of artificial clay-bearing sandstone, *Geophysics*, *47*(11), 1593–1605.

Liu, G., J. J. Butler Jr., G. C. Bohling, E. Reboulet, S. Knobbe, and D. W. Hyndman (2009), A new method for high-resolution characterization of hydraulic conductivity, *Water Resour. Res.*, *45*, W08202, doi:10.1029/2009WR008319.

Liu, G., C. Zheng, G. R. Tick, J. J. Butler Jr., and S. M. Gorelick (2010a), Relative importance of dispersion and rate-limited mass transfer in highly heterogeneous porous media: Analysis of a new tracer test at the Macrodispersion Experiment (MADE) site, *Water Resour. Res.*, *46*, W03524, doi:10.1029/2009WR008430.

Liu, J., M. Zhang, and C. Zheng (2010b), Role of ethics in groundwater management, *Ground Water*, *48*(1), 1, doi:10.1111/j.1745-6584.2009.00611.x.

Liu, G., S. Knobbe, and J. J. Butler Jr. (2013), Resolving centimeter-scale flows in aquifers and their hydrostratigraphic controls, *Geophys. Res. Lett.*, *40*, 1098–1103, doi:10.1002/grl.50282.

Ma, R., and C. Zheng (2011), Not all mass transfer rate coefficients are created equal, *Ground Water*, *49*(6), 772–774, doi:10.1111/j.1745-6584.2011.00822.x.

Major, E., D. A. Benson, J. Revielle, H. Ibrahim, A. Dean, R. M. Maxwell, E. Poeter, and M. Dogan (2011), Comparison of Fickian and temporally nonlocal transport theories over many scales in an exhaustively sampled sandstone slab, *Water Resour. Res.*, *47*, W10519, doi:10.1029/2011WR010857.

Nelson, P. H. (1994), Permeability-porosity relationships in sedimentary rocks, *The Log Analyst*, *35*(3), 38–62.

Neuman, S. P., and V. Di Federico (2003), Multifaceted nature of hydrogeologic scaling and its interpretation, *Rev. Geophys.*, *41*(3), 1014, doi:10.1029/2003RG000130.

Neuman, S. P., and D. M. Tartakovsky (2009), Perspective on theories of non-Fickian transport in heterogeneous media, *Adv. Water Resour.*, *32*(5), 670–680, doi:10.1016/j.advwatres.2008.08.005.

Nimmo, J. R. (2004), Porosity and pore size distribution, in *Encyclopedia of Soils in the Environment*, vol. 3, edited D Hillel, pp. 295–303, Elsevier, London, U. K.

Rao, P. S. C., R. E. Jessup, D. E. Rolston, J. M. Davidson, and D. P. Kilcrease (1980a), Experimental and mathematical description of nonadsorbed solute transfer by diffusion in spherical aggregates, *Soil Sci. Soc. Am. J.*, *44*, 684–688.

Rao, P. S. C., D. E. Rolston, R. E. Jessup, and J. M. Davidson (1980b), Solute transport in aggregated porous media: Theoretical and experimental evaluation, *Soil Sci. Soc. Am. J.*, *44*(6), 1139–1146.

Rao, P. S. C., R. E. Jessup, and T. M. Addiscott (1982), Experimental and theoretical aspects of solute diffusion in spherical and nonspherical aggregates, *Soil Sci.*, *133*(6), 342–349.

Reeves, D., D. A. Benson, and M. M. Meerschaert (2008), Transport of conservative solutes in simulated fracture networks: 1. Synthetic data generation, *Water Resour. Res.*, *44*, W05404, doi:10.1029/2007WR006069.

Revil, A., and L. Cathles (1999), Permeability of shaly sands, *Water Resour. Res.*, *35*(3), 651–662, doi:10.1029/98WR02700.

Revil, A., and N. Florsch (2010), Determination of permeability from spectral induced polarization in granular media, *Geophys. J. Int.*, 1480–1498, doi:10.1111/j.1365-246X.2010.04573.x.

Revil, A., P. A. Pezard, and P. W. J. Glover (1999), Streaming potential in porous media 1. Theory of the zeta potential, *J. Geophys. Res.*, *104*(B9), 20,021–20,031, doi:10.1029/1999JB900089.

Salamon, P., D. Fernàndez-Garcia, and J. J. Gómez-Hernández (2007), Modeling tracer transport at the MADE site: The importance of heterogeneity, *Water Resour. Res.*, *30*, W08404, doi:10.1029/2006WR005522.

Scheibe, T. D., Z. Hou, B. J. Palmer, and A. M. Tartakovsky (2013), Pore-scale simulation of intragranular diffusion: Effects of incomplete mixing on macroscopic manifestations, *Water Resour. Res.*, *49*, 4277–4294, doi:10.1002/wrcr.20333.

Schumer, R., D. A. Benson, M. M. Meerschaert, and B. Baeumer (2003), Fractal mobile/immobile solute transport, *Water Resour. Res.*, *39*(10), 1296, doi:10.1029/2003WR002141.

Schwarz, G. (1962), A theory of the low-frequency dielectric dispersion of colloidal particles in electrolyte solution, *J. Phys. Chem.*, *66*(12), 2636–2642.

Sen, P. N., C. Scala, and M. H. Cohen (1981), A self-similar model for sedimentary rocks with application to the dielectric constant of fused glass beads, *Geophysics*, *46*(5), 781–795, doi:10.1190/1.1441215.

Senturia, S. D., and J. D. Robinson (1970), Nuclear spin-lattice relaxation of liquids confined in porous solids, *Soc. Pet. Eng. J.*, *10*(3), 237–244.

Singha, K., F. D. Day-Lewis, and J. W. Lane Jr. (2007), Geoelectrical evidence of bicontinuum transport in groundwater, *Geophys. Res. Lett.*, *34*, L12401, doi:10.1029/2007GL030019.

Singha, K., L. Li, F. D. Day-Lewis, and A. B. Regberg (2011), Quantifying solute transport processes: Are chemically ''conservative'' tracers electrically conservative?, *Geophysics*, *76*(1), F53.

Slater, L. (2007), Near surface electrical characterization of hydraulic conductivity: From petrophysical properties to aquifer geometries: A review, *Surv. Geophys.*, *28*(2-3), 169–197, doi:10.1007/s10712-007-9022-y.

Slater, L., and D. P. Lesmes (2002), Electrical-hydraulic relationships observed for unconsolidated sediments, *Water Resour. Res.*, *38*(10), 1213, doi:10.1029/2001WR001075.

Straley, C., A. Matteson, S. Feng, L. M. Schwartz, W. E. Kenyon, and J. R. Banavar (1987), Magnetic resonance, digital image analysis, and permeability of porous media, *Appl. Phys. Lett.*, *51*(15), 1146–1148.

Swanson, R. D., K. Singha, F. D. Day-Lewis, A. Binley, K. Keating, and R. Haggerty (2012), Direct geoelectrical evidence of mass transfer at the laboratory scale, *Water Resour. Res.*, *48*, W10543, doi:10.1029/2012WR012431.

Timur, A. (1969), Pulsed nuclear magnetic resonance studies of porosity, movable fluid, and permeability of sandstones, *JPT J. Pet. Technol.*, *21*(6), 775–786.

Titov, K., A. Tarasov, Y. Ilyin, N. Seleznev, and A. Boyd (2010), Relationships between induced polarization relaxation time and hydraulic properties of sandstone, *Geophys. J. Int.*, *180*(3), 1095–1106, doi:10.1111/j.1365-246X.2009.04465.x.

Valckenborg, R., L. Pel, and K. Kopinga (2001), Cryoporometry and relaxometry of water in silica-gels, *Magn. Reson. Imaging*, *19*(3-4), 489–491.

van Genuchten, M. T., and P. J. Wierenga (1976), Mass transfer studies in sorbing porous media: I. Analytical solutions, *Soil Sci. Soc. Am. J.*, *40*(4), 473–480.

Walsh, J. B., and W. F. Brace (1984), The effect of pressure on porosity and the transport properties of rock, *J. Geophys. Res.*, *89*(B11), 9425–9431, doi:10.1029/JB089iB11p09425.

Wempe, W., and G. Mavko (2001), Three distinct porosity domains defined physically, hydraulically, electrically, and elastically, *Lead. Edge*, *20*(2), 198–207, doi:10.1190/1.1438912.

Westphal, H., I. Surholt, C. Kiesl, H. F. Thern, and T. Kruspe (2005), NMR measurements in carbonate rocks: Problems and an approach to a solution, *Pure Appl. Geophys.*, *162*(3), 549–570, doi:10.1007/s00024-004-2621-3.

Whittall, K. P., M. J. Bronskill, and R. M. Henkelman (1991), Investigation of analysis techniques for complicated NMR relaxation data, *J. Magn. Reson.*, *234*(95), 221–234.

Wood, W. W., T. F. Kraemer, and P. P. Hearn Jr. (1990), Intragranular diffusion: An important mechanism influencing solute transport in clastic aquifers?, *Science*, *247*(4950), 1569–1572.

Young, D. F., and W. P. Ball (1995), Effects of column conditions on the first-order rate modeling of nonequilibrium solute breakthrough, *Water Resour. Res.*, *31*(9), 2181–2192, doi:10.1029/95WR01612.

Zhang, X., and M. A. Knackstedt (1995), Direct simulation of electrical and hydraulic tortuosity in porous solids, *Geophys. Res. Lett.*, *22*(17), 2333–2336, doi:10.1029/95GL02230.

Zhang, Y., D. A. Benson, and D. M. Reeves (2009), Time and space nonlocalities underlying fractional-derivative models: Distinction and literature review of field applications, *Adv. Water Resour.*, *32*(4), 561–581, doi:10.1016/j.advwatres.2009.01.008.

Zheng, C., M. Bianchi, and S. M. Gorelick (2010), Lessons learned from 25 years of research at the MADE site, *Ground Water*, *49*(5), 1–14, doi:10.1111/j.1745-6584.2010.00753.x.

Zimmermann, E., A. Kemna, J. Berwix, W. Glaas, H. M. Münch, and J. A. Huisman (2008), A high-accuracy impedance spectrometer for measuring sediments with low polarizability, *Meas. Sci. Technol.*, *19*(10), 105603, doi:10.1088/0957-0233/19/10/105603.

Zinn, B., L. C. Meigs, C. F. Harvey, R. Haggerty, W. J. Peplinski, and C. F. Von Schwerin (2004), Experimental visualization of solute transport and mass transfer processes in two-dimensional conductivity fields with connected regions of high conductivity, *Environ. Sci. Technol.*, *38*(14), 3916–3926.

Zisser, N., A. Kemna, and G. Nover (2010), Dependence of spectral-induced polarization response of sandstone on temperature and its relevance to permeability estimation, *J. Geophys. Res.*, *115*, B09214, doi:10.1029/2010JB007526.